



In situ ultrasonic force signals during low-temperature thermosonic copper wire bonding

A. Shah^{a,*}, M. Mayer^a, Y. Zhou^a, S.J. Hong^b, J.T. Moon^b

^aMicrojoining Laboratory, University of Waterloo, ON, Canada

^bMK Electron Co., Ltd., Yongin, South Korea

ARTICLE INFO

Article history:

Received 10 November 2007

Accepted 12 May 2008

Available online 11 June 2008

Keywords:

Wire bonding

Ultrasonic

Thermosonic

Piezo-resistive

Microsensor

Bonding mechanism

Ball bonding

ABSTRACT

Ultrasonic in situ force signals from integrated piezo-resistive microsensors were used previously to describe the interfacial stick-slip motion as the most important mechanism in thermosonic Au wire ball bonding to Al pads. The same experimental method is applied here with a hard and a soft Cu wire type. The signals are compared with those obtained from ball bonds with standard Au wire. Prior to carrying out the microsensor measurements, the bonding processes are optimized to obtain consistent bonded ball diameters of 60 μm yielding average shear strengths of at least 110 MPa at a process temperature of 110 °C. The results of the process optimization show that the shear strength c_{pk} values of Cu ball bonds are almost twice as large as that of the Au ball bonds. The in situ ultrasonic force during Cu ball bonding process is found to be about 30% higher than that measured during the Au ball bonding process. The analysis of the microsensor signal harmonics leads to the conclusion that the stick-slip frictional behavior is significantly less pronounced in the Cu ball bonding process. The bond growth with Cu is approximately 2.5 times faster than with Au. Ball bonds made with the softer Cu wire show higher shear strengths while experiencing about 5% lower ultrasonic force than those made with the harder Cu wire.

© 2008 Elsevier B.V. All rights reserved.

1. Introduction

The thermosonic gold wire bonding process is the most widely used method for making interconnections in semiconductor packaging. Research and development in this area is driven by factors such as miniaturization, better performance, higher reliability, manufacturing speed up, and lower costs. One possible way to address these demands is to develop new wire materials. Cu wire has been considered as an alternative to Au because of better mechanical and electrical properties, and lower cost. However, the harder Cu free air ball generally requires application of higher normal and ultrasonic forces which increases the risk of underpad damage. To develop the best possible ball bonding processes with novel copper wires, an understanding of the bonding mechanisms with such wires promises to be helpful.

One of the most suitable methods to this end is to use microsensors to measure the in situ forces caused by the ultrasound induced to the pad during bonding. The Au ball bond on Al pad bonding process was characterized using piezo-resistive microsensors [1–3]. Based on the harmonics of the recorded ultrasonic signal, five bond phases are distinguished during the process. The third harmonic of the ultrasonic force signal was used to explain two

friction processes during the ball bonding of Au on Al pads: interfacial stick-slip friction between the Au ball and Al pad before and during bond formation, and friction between ball and capillary after bond formation [4,6]. It is concluded that the relative stick-slip motion between the ball and the pad includes wear which is a pre-requisite for high quality Au ball bonding on Al pads.

The concept of stick-slip friction was further developed in [7] to calculate the friction power delivered to the bond. In [8], a bond quality factor is introduced based on friction power. This model was extended in [9] to include wire deformation during the process.

In this paper, we report Au and Cu ball bonding process optimization and microsensor signals of ball bonding with Au and Cu wires on Al pads. Cu ball bonds are investigated for the same or similar mechanisms observed previously with Au wire. A comparison of the in situ signals obtained with two Cu wire types having different hardnesses is given.

2. Experimental

Thermosonic ball-wedge bonding is performed using a fully automatic ESEC 3100 wire bonder manufactured by Oerlikon ESEC, Cham, Switzerland, with a nominal ultrasonic frequency of 128 kHz. The bonding is performed using a standard Au wire, a soft Cu wire (Cu-S), and a hard Cu wire (Cu-H), all 25 μm (1 mil) in

* Corresponding author. Tel.: +1 519 888 4567x33326; fax: +1 519 888 6197.

E-mail addresses: ashah011@engmail.uwaterloo.ca (A. Shah), shah.aashish@gmail.com (A. Shah).

diameter and provided by MK Electron Co. Ltd., Yongin, Korea. Table 1 shows the basic mechanical properties of the three wire types. The values given as Vicker's hardness were measured on wire cross-sections made perpendicular to the wire main axis. Using the deformability characterization method reported in [10], it is found that the free air ball (FAB) made with Cu–S wire is softer than that made with Cu–H wire.

Table 1
Wire properties

| Property | Au | Cu–H | Cu–S |
|--------------------|------|------|------|
| Breaking load (gf) | 10.0 | 12.6 | 10.1 |
| Elongation (%) | 2.8 | 14.9 | 11.2 |
| Vicker's hardness | 50.0 | 57.8 | 55.5 |

Table 2
Nominal wedge bonding parameters

| Wire | Impact force (mN) | Bond force (mN) | Ultrasound (%) | Bond time (ms) | Pre-ultrasound, off at impact (%) |
|------|-------------------|-----------------|----------------|----------------|-----------------------------------|
| Au | 700 | 350 | 65 | 25 | 0 |
| Cu–H | 700 | 700 | 80 | 65 | 30 |
| Cu–S | 900 | 600 | 75 | 65 | 30 |

Table 3
EFO parameters to obtain a 50 μm diameter FAB

| Wire | E–W distance (μm) | Time (ms) | Tail length (μm) | Current (mA) |
|------|--------------------------------|-----------|-------------------------------|--------------|
| Au | 550 | 0.4 | 500 | 54.8 mA |
| Cu–H | | | | 83.1 mA |
| Cu–S | | | | 83.9 mA |

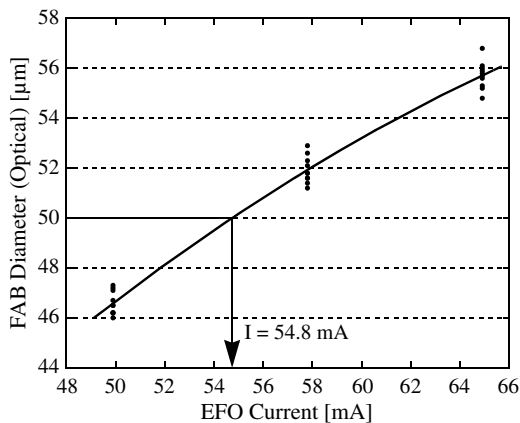


Fig. 1. FAB diameter vs. EFO current for Au wire. Thick solid line in center is parabolic fit. EFO time: 0.4 ms.

Bonding is performed at a nominal heater plate temperature of 125 °C resulting in actual chip temperature of about 110 °C. A commercial ceramics capillary having a hole diameter of 35 μm and a chamfer diameter of 51 μm is used. During the formation of FABs with Cu–H and Cu–S wires, a homogeneous mixture of 5% hydrogen and 95% nitrogen serves as shielding gas to prevent oxidation of the molten FAB metal during solidification. The flow rate of the shielding gas is set to 0.48 l/min.

2.1. Ball bonding process optimization

The wedge bonding parameters are optimized including an iterative method reported in [11], and shown in Table 2. These parameters result in symmetrical shapes without signs of fish tailing (peeling). The unit “%” is used for the ultrasonic parameter, where 1% is equivalent to a peak to peak vibration amplitude of 26.6 nm measured at the center of the transducer tip.

Next, the parameters for the electrical flame off (EFO) process are optimized to obtain a 50 μm diameter FAB. To this end, 30 FABs are made with three different levels of EFO current by fixing all other EFO parameters such as tail length, EFO time and electrode-wire (E–W) distance to those indicated in Table 3. The FAB diameters are measured using an optical microscope and fitted with a second order polynomial against the EFO current. From the fitted curve, the EFO current corresponding to a 50 μm FAB is determined. An example plot visualizing this procedure is shown in Fig. 1.

Table 3 shows the resulting EFO currents. Using this optimized EFO current, sample FABs are made as shown in Fig. 2a–c. The diameters are verified to be 50 μm with a standard deviation of less than 0.5 μm .

Previous studies using Au [12] and Cu [13,14] wires reported the use of double-load bonding processes to reduce defects related to bonding stress (e.g. cratering). In such a process, an impact force (pre-load) which is two to three times higher than the bonding force is used. In this study an impact force nominally three times as high as the subsequent bond force is programmed. Ultrasound is present only after the impact. The nominal ball bond parameters are given in Table 4. To verify the nominal impact to bond force ratio, the actual forces applied by the machine are recorded in real-time by the proximity sensor attached to the wire clamp of the bonder [11]. Example force profiles are shown in Fig. 3a–c. It is observed that the actual ratio is about 2.4. This variation between nominal and actual values may be attributed to universal mechanical limitations of controlling an impact event with the FAB plastically deformed.

The impact force values were adjusted such that the ball geometries were the same with each of the three wires with a target bonded ball diameter measured at the capillary imprint (BDC) of 60 μm . The nominal bonding force is then calculated to maintain the ratio described before.

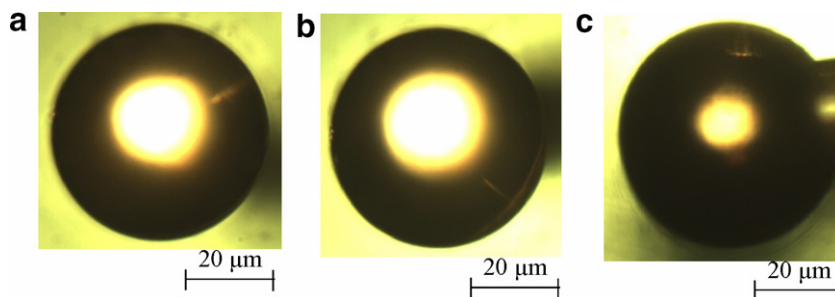


Fig. 2. Optical micrographs of example FABs obtained with (a) Au, (b) Cu–H, and (c) Cu–S wires.

Table 4
Nominal ball bonding parameters

| Wire | Bond time (ms) | Impact force (mN) | Bond force (mN) | Ultrasound (%) |
|------|----------------|-------------------|-----------------|----------------|
| Au | 25 | 800 | 266 | 24–65 |
| Cu–H | 25 | 1200 | 400 | 40–80 |
| Cu–S | 25 | 1200 | 400 | 42–80 |

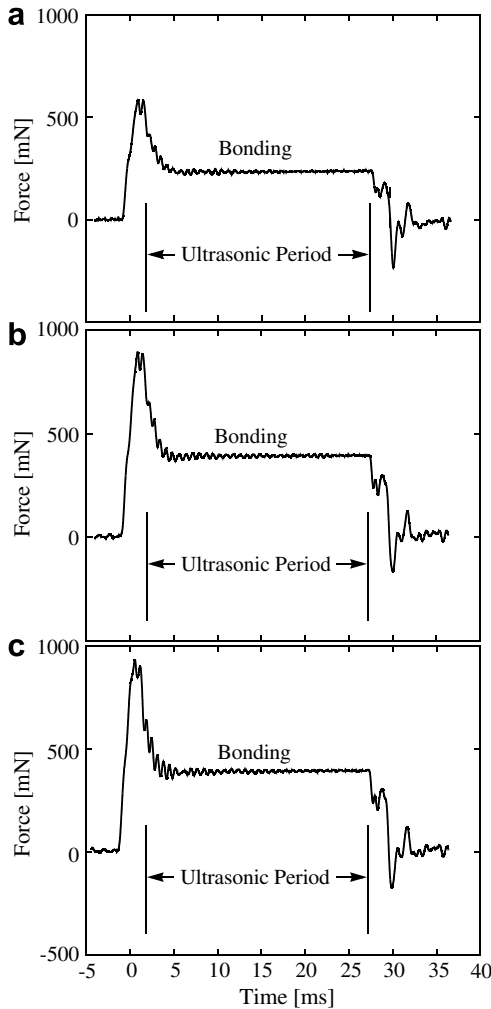


Fig. 3. Typical measured force profiles of (a) Au, (b) Cu–H, and (c) Cu–S ball bonding process.

The bonding time parameter describes the duration of ultrasound. Relatively long times of 25 ms were chosen to cover eventual process mechanisms occurring later during bonding. The chips with Al metallized bond pads used for the tests were supplied by Oerlikon Esec, Cham, Switzerland. An example is shown in Fig. 4 mounted on a PLCC44 lead frame. On each chip, ball bonding is performed by varying the ultrasound from the minimum ultrasound required to avoid ball non-stick on pad (NSOP), in steps to high ultrasound when the ball is heavily deformed. For levels lower than the ranges specified in Table 4 NSOPs are observed.

The bonds are repeated on 10 chips. BDC and ball height (BH) values are measured at the capillary imprint using an optical microscope. Then the balls are sheared, and the shear force (SF) is recorded. It is observed that during the shearing of Cu ball bonds, fracture occurred at the Cu–Al interface, while for Au ball bonds, failure occurred in the Au ball.

The shear strength (SS) of the ball bond is defined as the shear force divided by the cross-sectional area A , where $A = \pi (BDC/2)^2$.

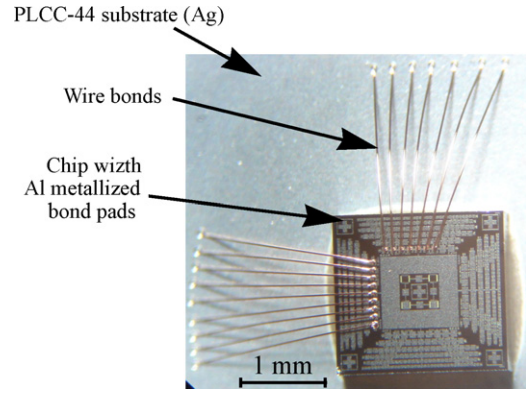


Fig. 4. Test chip used for ball bonding process optimization.

The variations of BDC, BH, and SS as a function of ultrasound are plotted in Figs. 5–7, for the processes with Au, Cu–H, and Cu–S wires, respectively. The optimum ultrasound levels are selected at the point when a sharp increase in BDC and decrease in BH is observed. This is the maximum ultrasound at which there is no *ultrasound enhanced deformation* (UED) [9], i.e. the ball deformation is due to the normal impact force alone. The values for the processes with Au, Cu–H, and Cu–S wires are 42%, 63%, and 58%, respectively, as indicated by the arrows in Fig. 5.

Ball bonds made with Cu wires have higher shear strength than those made with Au wire. This is consistent with the findings reported in [15]. One of the reasons for this higher shear strength is possibly the higher ultrasound stress supported by Cu without yielding. If the ultrasound stress induced to the ball is larger than the yield strength, additional UED occurs, and the bonded ball dimensions are out of specification. Since Cu has a tensile strength of about 210 MPa which is higher than that of Au (120 MPa) [18], higher ultrasound levels can be used without UED, resulting in higher shear strengths.

In order to quantify the process capability (i.e. the ability of the process to produce output within specification limits), the c_{pk} value is calculated using Eq. (1) [17]

$$c_{pk} = \frac{\mu - LSL}{3\sigma} \quad (1)$$

where μ , LSL , and σ are the average, lower specification limit, and standard deviation of the ball bond shear strength, respectively. From the EIA/JEDEC Standard 22-B116 [16], LSL is defined to be 65.2 MPa.

The c_{pk} values are determined for various ultrasound levels for each of the three wire types and plotted in Fig. 7a–c, respectively, together with parabolic curves fitted to the c_{pk} values. Typical c_{pk} values estimated from the fits are 2 for Au and between 4 and 5 for the Cu wires.

To obtain a shear strength equivalent to that reached with Au ball bonds (≈ 110 MPa), Cu ball bonds can be made at ultrasound levels lower than optimum. A lower ultrasound level leads to a reduction of the stress induced to the pad during bonding, thereby reducing the chances of underpad damage.

To characterize the bond growth, ball bonds are made with Au, Cu–H, and Cu–S wires using the respective optimized settings with bond time parameters varying in steps of at least 1 ms and not smaller than 2.5 ms. The tests are conducted on five chips on the daisy chain pads shown in Fig. 8. For each bond time, two bonds are made on each chip. The shear strengths for various bond time parameters are shown in Fig. 9.

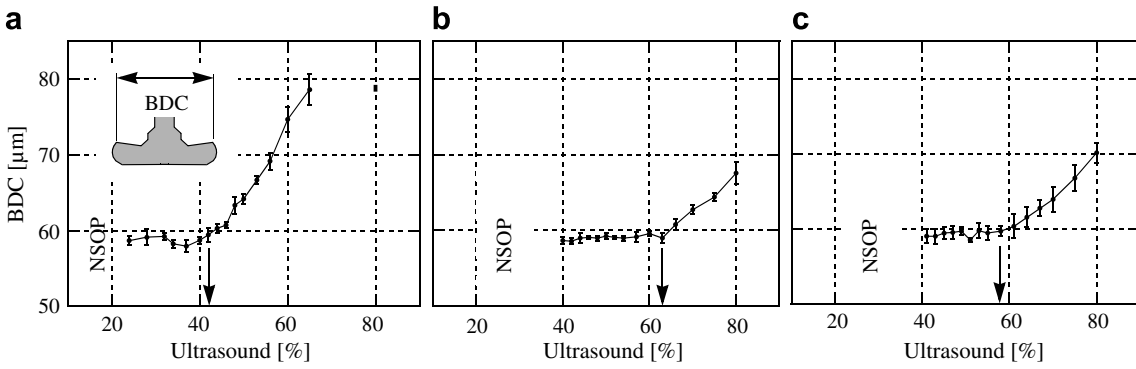


Fig. 5. Bonded ball diameter vs. ultrasound for (a) Au, (b) Cu-H, and (c) Cu-S wires.

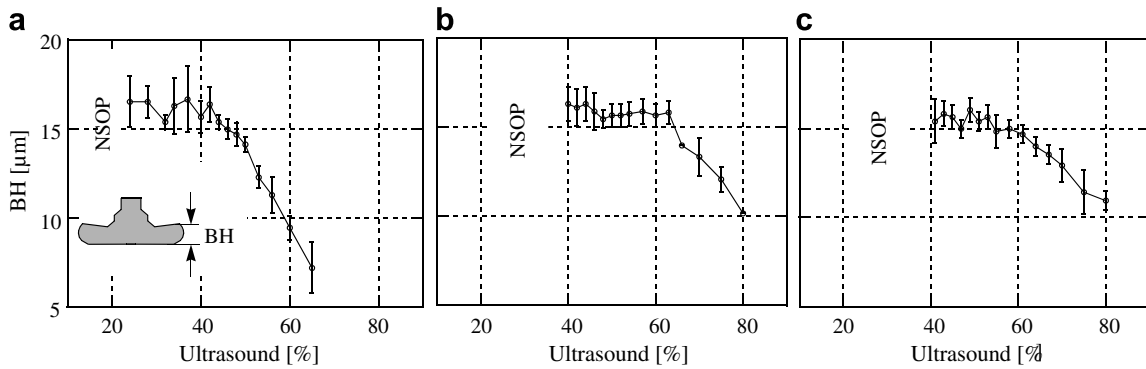


Fig. 6. Bonded ball height vs. ultrasound for (a) Au, (b) Cu-H, and (c) Cu-S wires.

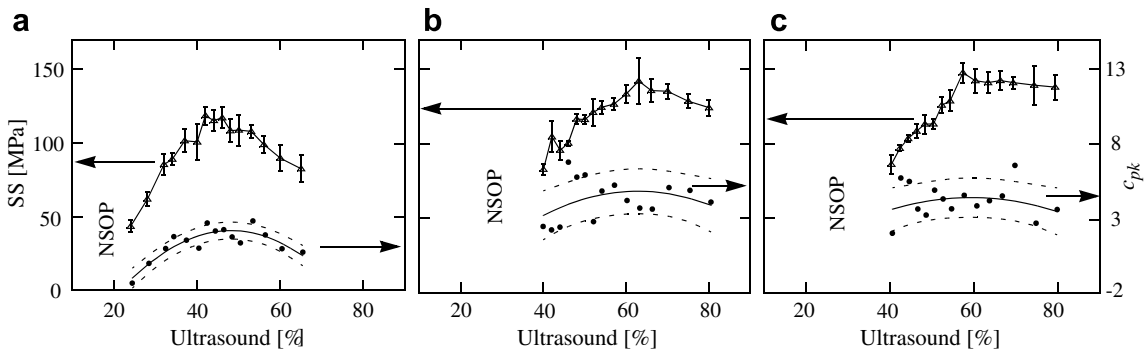


Fig. 7. Ball shear strength and c_{pk} values with a parabolic fit (dashed lines indicate ± 1 standard deviation) vs. ultrasound for (a) Au, (b) Cu-H, and (c) Cu-S wires.

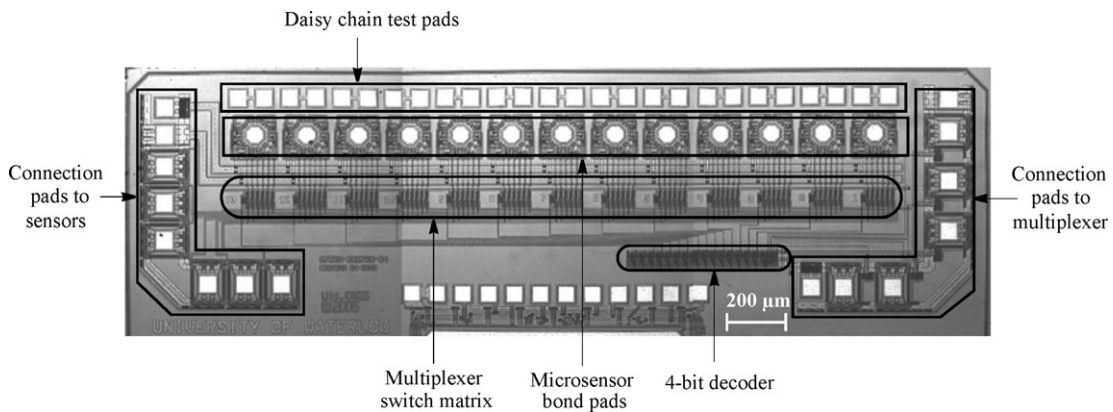


Fig. 8. Optical micrograph of a part of the test chip depicting the microsensors on the multiplexer.

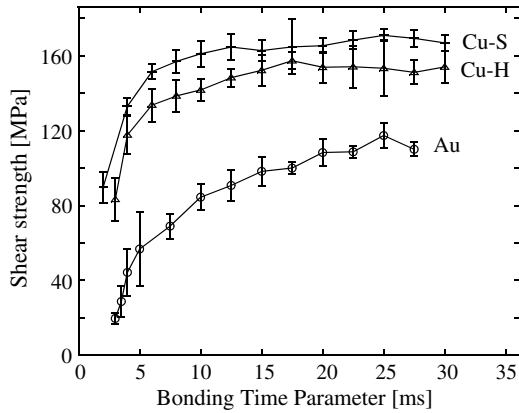


Fig. 9. Shear strength vs. bonding time plots for Au, Cu-H, and Cu-S ball bonds. Results shown only for parameters without NSOP occurring.

2.2. Microsensor measurements

A test chip was designed by the Microjoining Laboratory of the University of Waterloo, Ontario, Canada, and manufactured using a 0.7 μm CMOS process of AMI Semiconductor, Oudenaarde, Belgium. It contains thirteen bonding pads with integrated microsensors shown in Fig. 8 which are addressed using a multiplexing circuit co-integrated on the chip. The microsensor is made up of four n⁺ diffused piezo-resistors (sensor elements) in a Wheatstone bridge configuration illustrated in Fig. 11a and b, connected to a bus by high temperature switches, and selectively sensitive to the forces in ultrasound direction. An example bond on the octagonal shaped test pad between the sensing elements of the microsensor is shown by the SEM micrograph in Fig. 10. The multiplexer is composed of a switch matrix and a 4-bit decoder. The principle, design, and operation of such microsensors are described in detail in [4,5].

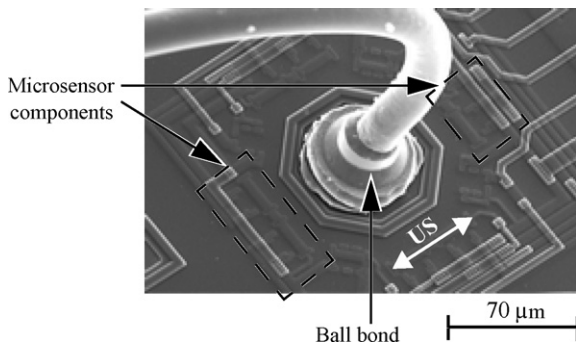


Fig. 10. SEM micrograph of a ball bond on the microsensor test pad (shown here is an optimized ball bond performed using Cu-S wire).

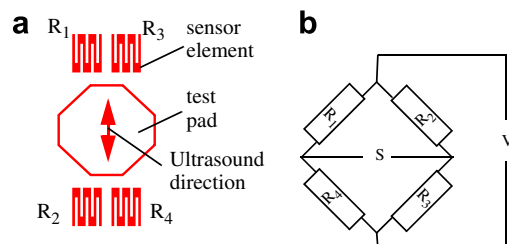


Fig. 11. Illustration of microsensor (a) element shape and location (not to scale), and (b) electrical diagram, V is supply voltage, S is sensor signal.

The test chip is mounted on a gold plated polyimide substrate supplied by Oerlikon Esec, Cham, Switzerland, using silver filled epoxy cured in an oven at 150 °C for 90 min. The sensor channels and the multiplexer addressing channels are connected to the terminals on the substrate by gold wire bonds as shown in Fig. 12. The design and operation of the measurement system is reported in [4,5]. A DC voltage of 3 V is applied to the sensor. Ball bonding

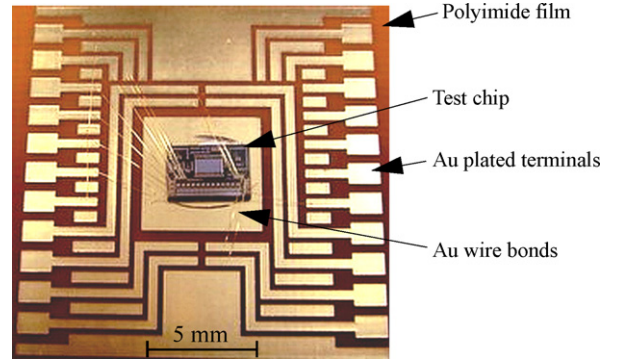


Fig. 12. Microsensor chip on substrate. Au wire bonds connecting the connection pads to substrate terminals.

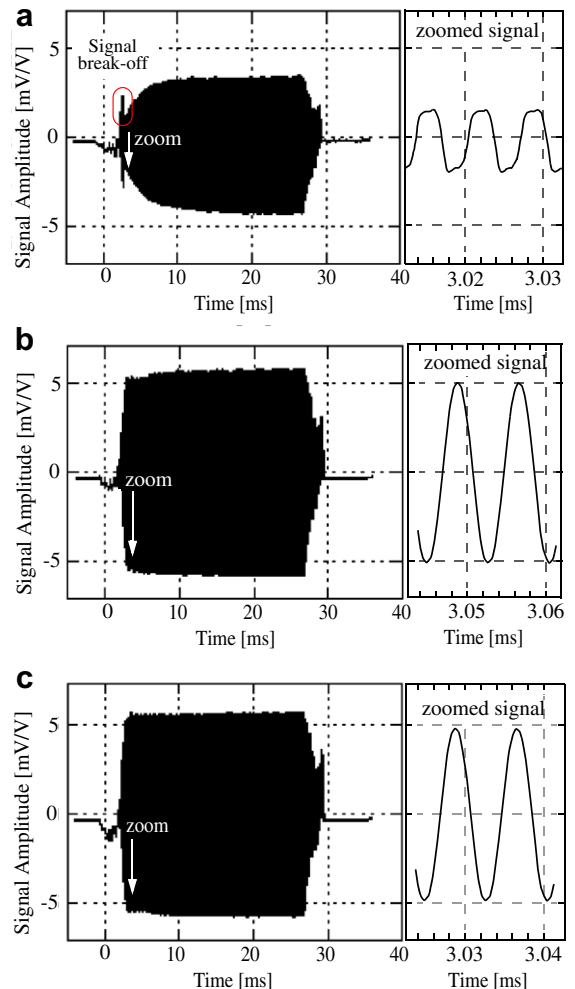


Fig. 13. (a) Ultrasonic microsensor force signals of (a) Au, (b) Cu-H, and (c) Cu-S ball bonds.

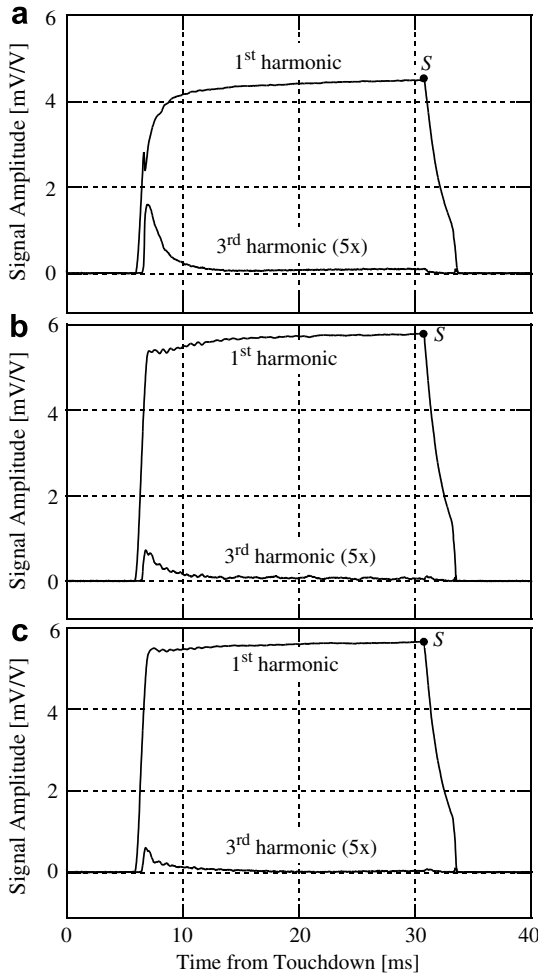


Fig. 14. Amplitudes of harmonics from ultrasonic microsensor force signals of (a) Au, (b) Cu-H, and (c) Cu-S ball bonds.

using the optimized parameters is performed on the test pads with each of the three wires, and the real-time signals of the microsensor are recorded on a PC. The measurements are performed on three test chips. On each test chip, three ball bonding measurements are recorded with each of the three wires to make a sample of nine measurements per wire type spread over the three chips. The signals are shown in Fig. 13a–c, respectively. They consist of approximately 3125 cycles of ultrasonic vibration. Hence, the signals appear to be filled areas. The waveform of the signal between 3 and 4 ms after touchdown is shown adjacent to the signal for each wire type.

The harmonics of the microsensor signals obtained with Au, Cu-H, and Cu-S wires are shown in Fig. 14a–c, respectively. The results obtained with Au wire are consistent with those reported previously [1–8]. Between 1 ms and 1.5 ms after ultrasonic dissipation starts, a break-off in the microsensor signal is observed, characterized by a sharp fall in the first harmonic and a sharp rise in the third harmonic. During this period, the waveform of the signal becomes cropped as shown in Fig. 13a, indicating a harmonically driven stick-slip motion at the bond interface.

In contrast, in the Cu ball bonding process, as soon as the ultrasonic dissipation starts, the force signal rises rapidly and no signal break-off is observed. The relative amount of the third harmonic is approximately 5 times smaller than in the Au–Al ball bonding process, as shown by the amplitude ratios of the third by the first harmonic in Fig. 15. The cropped sinusoidal waveform explaining the interfacial stick-slip motion is not evident in the Cu ball bonding

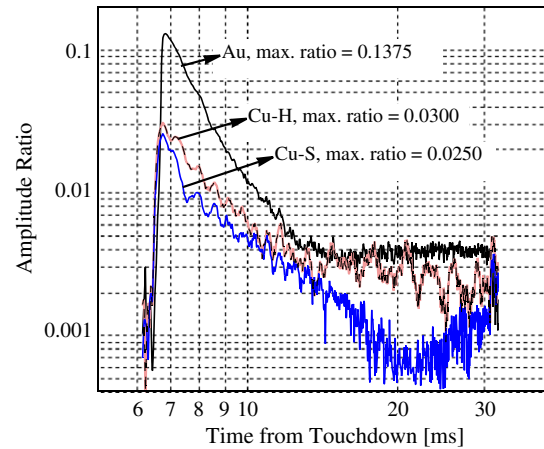


Fig. 15. Ratios of 3rd by 1st harmonic amplitudes vs. time.

process. While reduced in relative magnitude compared to the Au/Al process, the amount of stick-slip friction in the Cu/Al is still an important if not the leading mechanism for a successful Cu ball bond.

The maximum ultrasonic forces (at the point S in Fig. 14) with Au, Cu-H, and Cu-S wires are 4.46 ± 0.01 , 5.89 ± 0.01 , and 5.67 ± 0.02 mV/V, respectively. Thus, approximately 27–32% higher ultrasonic force is observed during the Cu ball bonding processes than during that with Au. The ultrasonic force observed with Cu-S is about 5% lower than that observed with Cu-H in contrast to the shear strength being higher with Cu-S (Fig. 9). A possible reason for this paradox is that Cu-S might have a higher reactivity when bonding with Al. Another reason might be that a softer Cu-S bonded ball distributes the stresses during the shear test more evenly across the interface, reducing stress peaks that initiate shear test fracture.

It is observed that the rate of bond growth in Cu is faster than in Au. When bonded with the smallest time parameter (rounded to integer millisecond values) required for successful bonding (no NSOP), Au reaches only about 20% of its maximum shear strength (Fig. 9), and the microsensor signal (Fig. 14a) is at 73% of its maximum value. The microsensor signal and the shear strength reach 90% of their maximum values at 2.9 ms and 16 ms after ultrasound on, respectively. In contrast, the bond with Cu wire reaches 50% of its maximum shear strength (Fig. 9), when bonded with the smallest time parameter (rounded to integer millisecond values), and the microsensor signal (Fig. 14b and c) is 94% of its maximum level. The microsensor signal and the shear strength reach 90% of its maximum level 1.1 ms and 6 ms after ultrasound on, respectively.

3. Conclusions

1. The method using piezoresistive microsensors is fast and applicable to various wires, yielding robust and repeatable results of high resolution.
2. The ultrasonic tangential force observed with Cu wires is approximately 30% higher than that observed with Au wire.
3. The bond growth with Cu is approximately 2.5 times faster than that with Au.
4. The cropped sinusoidal waveform used to explain the stick-slip friction is not evident in Cu–Al ball bonding process.
5. The softer Cu FAB shows increased shear strength at about 5% lower ultrasonic force than the harder Cu FAB and therefore is recommended for low stress bonding on sensitive substrates such as low- k chips.

Acknowledgements

This work is supported by MK Electron Co. Ltd. (Yongin, South Korea), Microbonds Inc. (Markham, Ontario, Canada), Natural Sciences and Engineering Research Council of Canada (NSERC), and Ontario Centres of Excellence (OCE). Technical support of Oerlikon ESEC (Cham, Switzerland) is gratefully acknowledged.

References

- [1] M. Mayer, J. Schwizer, O. Paul, D. Bolliger, H. Baltes, In situ ultrasonic stress measurements during ball bonding using integrated piezoresistive microsensors, *Advances in Electronic Packaging* (Proc. InterPACK99 Conference), vol. 26-1, ASME, 1999, pp. 973–978.
- [2] M. Mayer, Microelectronic bonding process monitoring by integrated sensors, Ph.D. Dissertation ETH No. 13685, Physical Electronics Laboratory, ETH Zurich, Switzerland, 2000, ISBN 3-89649-620-4.
- [3] J. Schwizer, M. Mayer, D. Bolliger, O. Paul, H. Baltes, Thermosonic ball bonding: friction model based on integrated microsensor measurements, in: *Proceedings of the IEEE/CPMT International Electronics Manufacturing Technology Symposium*, 1999, pp. 108–114.
- [4] J. Schwizer, M. Mayer, O. Brand, *Force Sensors for Microelectronic Packaging Applications*, Springer-Verlag, Berlin, 2005.
- [5] J. Schwizer, Q. Fueglistaller, M. Mayer, M. Althaus, O. Brand, H. Baltes, MEMS system with multiplexer for in situ and real-time wire bonding diagnosis, in: *Proceedings of SEMI Technical Symposium, Advanced Packaging Technologies I*, SEMI Singapore, 2002, pp. 163–167.
- [6] J. Schwizer, CMOS force sensors for wire bonding and flip chip process characterization, Ph.D. Dissertation ETH No. 15293, Physical Electronics Laboratory, ETH Zurich, Switzerland, 2003.
- [7] M. Mayer, J. Schwizer, Ultrasonic bonding: understanding how process parameters determine the strength of Au–Al bonds, in: *Proceedings of IMAPS International Symposium on Microelectronics*, 2002.
- [8] M. Mayer, J. Schwizer, Thermosonic ball bonding model based on ultrasonic friction power, in: *Proceedings of the IEEE Electronic Packaging Technology Conference EPTC'03*, Singapore, 2003, pp. 738–743.
- [9] H. Gaul, M. Schneider-Ramelow, K.-D. Lang, H. Reichl, Predicting the shear strength of a wire bond using laser vibration measurements, in: *Proceedings of the 1st Electronics System Integration Technology Conference*, vol. 2, 2006, pp. 719–725.
- [10] C.J. Hang, I. Lum, J. Lee, M. Mayer, Y. Zhou, C.Q. Wang, S.J. Hong, S.M. Lee, Online hardness characterization of novel 2-mil copper bonding wires, in: *Proceedings of ASME InterPACK'07 Conference*, 2007.
- [11] J. Lee, M. Mayer, Y. Zhou, S.J. Hong, *Microelectron. J.* 38 (2007) 842–847.
- [12] R.G. McKenna, R.L. Mahle, High impact bonding to improve reliability of VLSI die in plastic packages, in: *Proceedings of the IEEE Electronic Components Conference*, 1989, pp. 424–427.
- [13] K. Toyozawa, K. Fujita, T. Minamide, T. Maeda, Development of copper wire bonding application technology, in: *Proceedings of the IEEE Electronic Components and Technology Conference*, 1990, pp. 762–767.
- [14] K. Toyozawa, K. Fujita, S. Minamide, T. Maeda, *IEEE Transactions on Components, Hybrids, and Manufacturing Technology* 13 (4) (1990) 667–672.
- [15] N. Srikanth, S. Murali, Y.M. Wong, C.J. Vath, *Thin Solid Films* 462–463 (2004) 339–345.
- [16] Wire Bond Shear Test Method, Electronics Industries Alliance/JEDEC Standard EIA/JESD22-B116, 1998, pp. 7–8.
- [17] D. Montgomery, *Introduction to Statistical Quality Control*, John Wiley and Sons, New York, 2004.
- [18] *ASM Handbook*, vol. 2, Properties and Selection: Nonferrous Alloys and Special Purpose Materials, 10th ed., ASM International, 1990.